Te 5*p* orbitals bring three-dimensional electronic structure to two-dimensional $Ir_{0.95}Pt_{0.05}Te_2$

D. Ootsuki,[1] T. Toriyama,[2] S. Pyon,[3] K. Kudo,[3] M. Nohara,[3] K. Horiba,[4] M. Kobayashi,[4] K. Ono,[4] H. Kumigashira,[4] T. Noda,[1] T. Sugimoto,[1] A. Fujimori,[5] N. L. Saini,[6] T. Konishi,[7] Y. Ohta,[2] and T. Mizokawa[1]

[1]*Department of Physics and Department of Complexity Science and Engineering, University of Tokyo, 5-1-5 Kashiwanoha, Chiba 277-8561, Japan*

[2]*Department of Physics, Chiba University, Inage-ku, Chiba 263-8522, Japan*

[3]*Department of Physics, Okayama University, Kita-ku, Okayama 700-8530, Japan*

[4]*Institute of Materials Structure Science, High Energy Accelerator Research Organization (KEK), Tsukuba, Ibaraki 305-0801, Japan*

[5]*Department of Physics, University of Tokyo, 7-3-1 Hongo, Tokyo 113-0033, Japan*

[6]*Department of Physics, University of Roma "La Sapienza" Piazzale Aldo Moro 2, 00185 Roma, Italy*

[7]*Graduate School of Advanced Integration Science, Chiba University, Inage-ku, Chiba 263-8522, Japan*

(Received 4 December 2013; revised manuscript received 21 February 2014; published 6 March 2014)

We have studied the nature of the three-dimensional multiband electronic structure in the two-dimensional triangular lattice $Ir_{1-x}Pt_xTe_2$ ($x = 0.05$) superconductor using angle-resolved photoemission spectroscopy (ARPES), x-ray photoemission spectroscopy (XPS), and a band structure calculation. ARPES results clearly show a cylindrical (almost two-dimensional) Fermi surface around the zone center. Near the zone boundary, the cylindrical Fermi surface is truncated into several pieces in a complicated manner with strong three dimensionality. The XPS result and the band structure calculation indicate that the strong Te 5*p*-Te 5*p* hybridization between the $IrTe_2$ triangular lattice layers is responsible for the three dimensionality of the Fermi surfaces and the intervening of the Fermi surfaces observed by ARPES.

DOI: 10.1103/PhysRevB.89.104506 PACS number(s): 74.70.Xa, 74.25.Jb, 71.30.+h, 71.20.−b

I. INTRODUCTION

3*d*, 4*d*, and 5*d* transition-metal compounds, and 5*f* actinide compounds with layered crystal structures, often exhibit three-dimensional multiband Fermi surfaces, which can induce complicated spin-charge-orbital instabilities due to the interplay between the two-dimensional electronic structure of the layer and the interaction between neighboring layers. The layered compounds tend to have flat cleavage surfaces which are suitable for angle-resolved photoemission spectroscopy (ARPES) measurements, and the three-dimensional electronic structures can be observed by sweeping photon energy for ARPES. For example, the ARPES study on the classical 1T-$TaSe_2$ system has shown that the large Se-Se interaction between the layers and the strong covalency between the Ta 5*d* and Se 4*p* orbitals provide three-dimensional Fermi surfaces, which play important roles in the charge density wave formation [1]. In the case of Fe-based superconductors, the origin of the spin and orbital order in the parent materials is still controversial and the three-dimensional multiband Fermi surfaces observed by ARPES are key ingredients to understand the spin and orbital instabilities as well as the nodeless and nodal superconducting states [2]. In addition, the recent ARPES study on URu_2Si_2 (which has the $ThCr_2Si_2$ structure) has revealed that the nesting vectors in the three-dimensional momentum space are associated with the "hidden" order [3].

Very recently, the layered 5*d* transition-metal chalcogenide $IrTe_2$ has been attracting great interest due to the discovery of superconductivity in doped or intercalated $IrTe_2$ by Pyon *et al.* [4] and Yang *et al.* [5]. $IrTe_2$ undergoes a structural phase transition at ∼270 K from the trigonal ($P\bar{3}m1$) to the monoclinic ($C2/m$) structure [6,7]. Since the Ir 5*d*-to-Te 5*p* charge-transfer energy is found to be small [8], the strong Ir 5*d*-Te 5*p* hybridization with the $IrTe_2$ layer and the Te 5*p*-Te 5*p* hybridization between the $IrTe_2$ layers can play significant roles in the structural phase transition as proposed by Fang *et al.* and Oh *et al.* [9,10]. In addition, band structure calculations predict that the multiband Fermi surfaces of undistorted and distorted $IrTe_2$ are three dimensional in spite of its layered structure [5,9]. Although the multiband electronic structure of the Ir 5*d* and Te 5*p* orbitals in $IrTe_2$ has been studied using ARPES [11], the three dimensionality of the Fermi surfaces has not been observed in $IrTe_2$ and its relatives. Here, fundamental questions to be addressed are (i) whether the triangular lattice $Ir_{1-x}Pt_xTe_2$ has the three-dimensional Fermi surfaces as predicted by the band structure calculation and (ii) what the characteristics are of the observed band structures in the triangular lattice $Ir_{1-x}Pt_xTe_2$. In the present study, we have performed ARPES measurements of $Ir_{0.95}Pt_{0.05}Te_2$ at various photon energies in order to study the three-dimensional Fermi surfaces of the undistorted triangular lattice superconductor $Ir_{1-x}Pt_xTe_2$.

II. EXPERIMENTAL AND CALCULATIONAL DETAILS

The single-crystal samples of $Ir_{0.95}Pt_{0.05}Te_2$ were prepared as reported in the literature [12]. The ARPES measurements were performed at beam line 28A of Photon Factory, KEK using a SCIENTA SES-2002 electron analyzer with circularly polarized light. The total energy resolution was set to 20–30 meV for the excitation energies from $h\nu = 79$ eV to $h\nu = 54$ eV. The base pressure of the spectrometer was in the 10^{-9} Pa range. The single crystals of $Ir_{0.95}Pt_{0.05}Te_2$, which were oriented by *ex situ* Laue measurements, were cleaved at 20 K under the ultrahigh vacuum and the spectra were acquired within 24 hours after the cleaving. The x-ray photoemission spectroscopy (XPS) measurement was carried out using the JEOL JPS9200 analyzer. Mg Kα (1253.6 eV) was used as the x-ray source. The total-energy resolution was set to ∼1.0 eV, and the binding energy was calibrated

using the Au $4f$ core level of the gold reference sample. For the band structure calculations, we employed the code WIEN2k [13] based on the full-potential linearized augmented-plane-wave method and present the calculated results obtained in the generalized gradient approximation (GGA) for electron correlations, where we used the exchange-correlation potential of Ref. [14]. The spin-orbit interaction was taken into account for both Ir and Te ions.

III. RESULT AND DISCUSSION

Before presenting the ARPES result, let us discuss the fundamental electronic structure of $Ir_{0.95}Pt_{0.05}Te_2$, which provides the three-dimensional Fermi surfaces in the layered triangular lattice material, based on the XPS result. In Fig. 1(a), the Ir $4f$ core-level XPS spectrum of $Ir_{0.95}Pt_{0.05}Te_2$ is compared with that of $CuIr_2S_4$. While the formal valence of Ir is $+4$ in $Ir_{0.95}Pt_{0.05}Te_2$, the binding energy of the Ir $4f$ core level is much lower than that of $CuIr_2S_4$ with $Ir^{3.5+}$, indicating that the actual valence of Ir should be smaller than $+3.5$. Therefore, some of the Te $5p$ electrons are transferred from the Ir $5d$ orbitals, and the Te $5p$ orbitals are expected to be partially unoccupied. This picture is consistent with the band structure calculation in which the electronic states near the Fermi level (E_F) have substantial Te $5p$ character. In addition, the binding energy of the Te $3d$ core level [Fig. 1(b)] is relatively small compared to other transition-metal tellurides, indicating that the Te $5p$ states are heavily involved in the near-E_F electronic states. Indeed, as shown in Fig. 1(c), the valence-band XPS spectra of $Ir_{0.95}Pt_{0.05}Te_2$ exhibit a peak around 2.5 eV below E_F, whereas the spectral weight near E_F is rather weak. Since the photoionization cross section of Ir $5d$ is much larger than that of Te $5p$ at this photon energy, the valence-band XPS result suggests that the electronic states that are 2–3 eV below E_F are dominated by Ir $5d$, while those that are near E_F have more Te $5p$ character.

Figures 2(a)–2(j) show the second derivative plots of ARPES spectra along the cuts approximately in the Γ-K or A-H direction taken at various photon energies from $h\nu =$ 79 eV to $h\nu = 54$ eV. Here, the momentum along the Γ-K

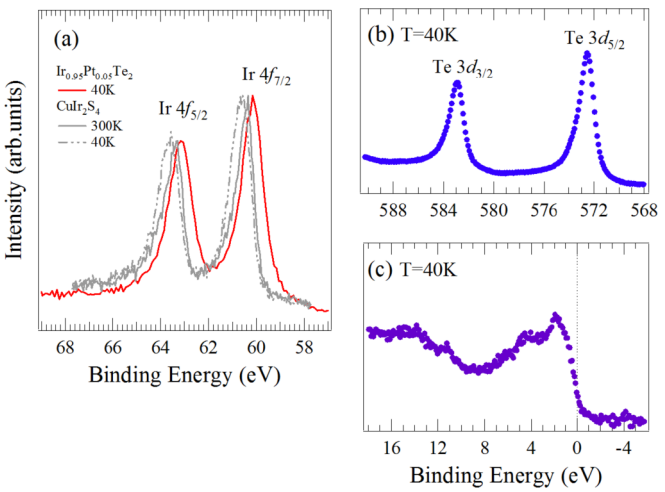

FIG. 1. (Color online) XPS spectra of $Ir_{0.95}Pt_{0.05}Te_2$ for the (a) Ir $4f$ core level, (b) Te $3d$ core level, and (c) valence band.

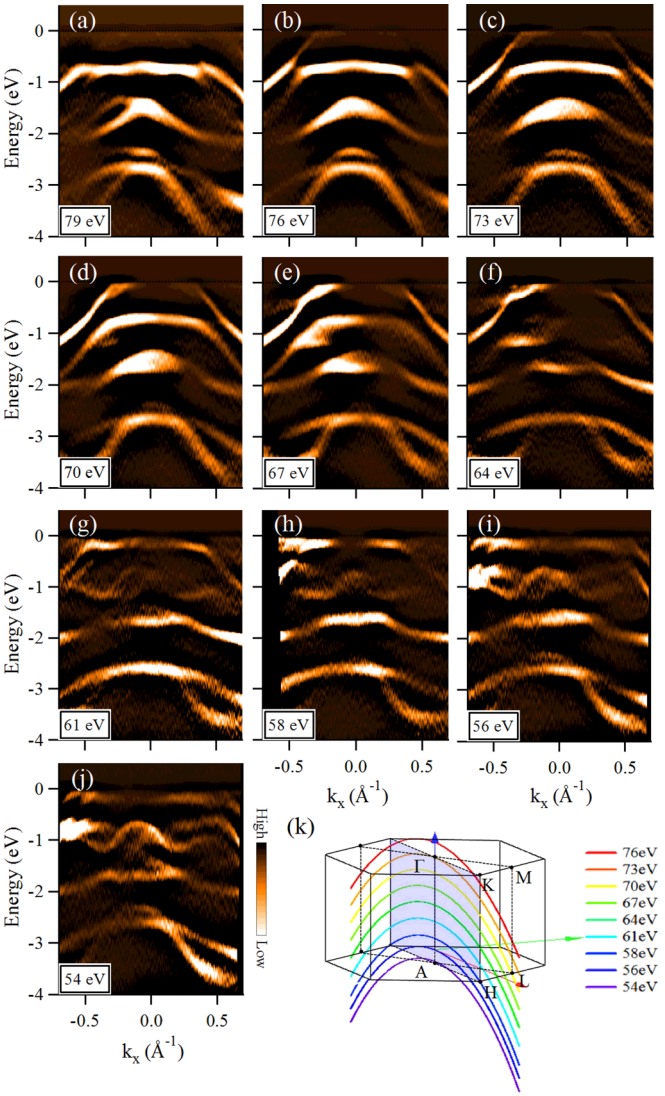

FIG. 2. (Color online) Second derivative plots of ARPES spectra along the cuts approximately in the Γ-K or A-H direction taken at $h\nu$ = (a) 79, (b) 76, (c) 73, (d) 70, (e) 67, (f) 64, (g) 61, (h) 58, (i) 56, and (j) 54 eV. (k) Direction of the cuts for various photon energies indicated in the Brillouin zone. The k_x-k_z curves are given by $k_z = 0.512 \times \sqrt{(h\nu - W)\cos^2\theta + V_0}$, where $\theta = \sin^{-1}[k_x/(0.512 \times \sqrt{h\nu - W})]$.

or A-H direction of the Brillouin zone of $IrTe_2$ is defined as k_x. The momentum along the Γ-A direction is k_z, and k_y is perpendicular to k_x and k_z. The relationship between k_x, k_y, and k_z is given by $h\nu - W + V_0 = \hbar^2/2m \times \sqrt{k_x^2 + k_y^2 + k_z^2}$ at photon energy of $h\nu$. Here, the work function W and V_0 are set to 4.4 and 14 eV, respectively. The momentum parallel to the surface is conserved at the electron emission from the surface and is measured as $\sqrt{k_x^2 + k_y^2} = 0.512 \times \sqrt{h\nu - W}\sin\theta$ (in unit of $Å^{-1}$), where θ is the emission angle from the surface normal direction. Therefore, the momentum perpendicular to the surface is given by $k_z = 0.512 \times \sqrt{(h\nu - W)\cos^2\theta + V_0}$, and the photon energy $h\nu$ can be translated into k_z. In Fig. 2(k), the direction of the cuts for various photon energies is indicated in the Brillouin zone.

As seen in Figs. 2(a)–2(j), the band dispersions above −1.5 eV strongly depend on the photon energy, whereas those below −1.5 eV are relatively insensitive to the photon energy. According to the band structure calculation, the band dispersions above −1.5 eV are mainly constructed from the Ir 5d t_{2g} and the Te 5p orbitals. Under the trigonal ligand field, the Ir 5d t_{2g} orbitals are split into the Ir 5d a_{1g} and Ir 5d e'_g orbitals whose lobes are directed to the out-of-plane (z-axis) direction and the in-plane (xy-plane) direction, respectively. The Ir 5d a_{1g} orbital (e'_g orbitals) strongly hybridize with the Te 5p_z (5p_x and 5p_y) orbitals, which have the larger (smaller) 5p-5p transfer integrals between the $IrTe_2$ layers. Therefore, the Ir 5d a_{1g}-Te 5p_z bands have three-dimensional band dispersion, while the Ir 5d e'_g-Te 5$p_{x,y}$ bands are expected to be two dimensional. This situation is roughly obtained in the band structure calculation without the spin-orbit interaction and is not consistent with the ARPES result. On the other hand, in the band structure calculation with the spin-orbit interaction, the Ir 5d a_{1g} and e'_g orbitals are heavily mixed due to the strong spin-orbit interaction of the Ir 5d orbitals, and all of the Ir 5d t_{2g}-Te 5p bands exhibit large three dimensionality. The photon-energy dependence of the observed band dispersions displayed in Fig. 2 shows that all of the Ir 5d t_{2g}-Te 5p bands near E_F strongly depend on k_z, consistent with the prediction of the band structure calculation considering the spin-orbit interaction.

In Fig. 3, the ARPES intensity at E_F is plotted as a function of k_x and k_z for various photon energies and is compared with the calculated Fermi surfaces indicated by the dots. The observed ARPES intensity at E_F roughly follows the calculated Fermi surfaces. In the region around the Γ point ($4.8\,\text{Å}^{-1} < k_z < 4.4\,\text{Å}^{-1}$), the observed Fermi surfaces are rather simple. The inner Fermi surface is almost parallel to the Γ-A axis, and the distance between the Γ-A axis and the inner Fermi surface is ∼0.25 Å^{-1}. In the region around the A point ($4.4\,\text{Å}^{-1} < k_z < 4.1\,\text{Å}^{-1}$), the inner and outer Fermi surfaces show the complicated structure. In particular, whereas the calculation predicts that the inner Fermi surfaces are broken

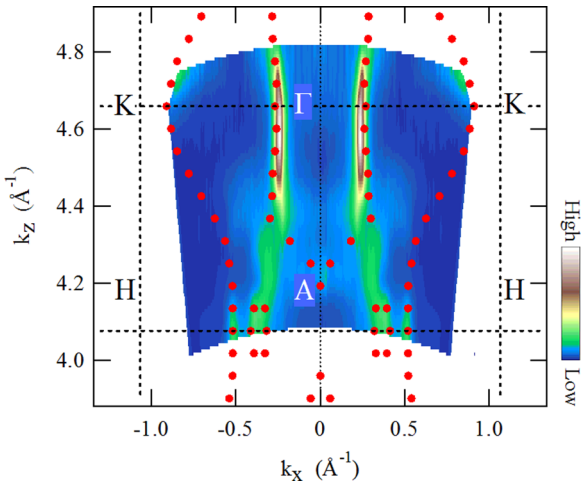

FIG. 3. (Color online) Fermi-surface map in the k_x-k_z plane. Here, k_x and k_z are electron momenta along the x direction (the Γ-K or A-H direction) and the z direction (the Γ-A direction), respectively.

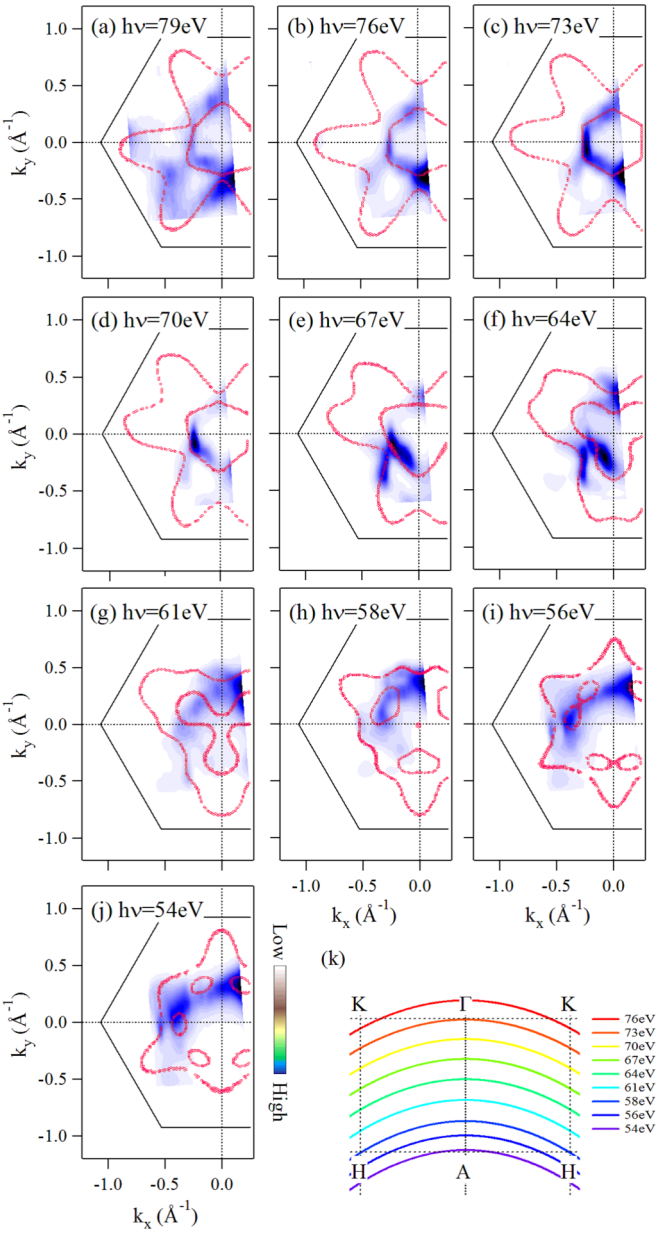

FIG. 4. (Color online) Fermi-surface maps in the k_x-k_y plane with (a) $k_z = 4.82$, (b) $k_z = 4.74$, (c) $k_z = 4.65$, (d) $k_z = 4.57$, (e) $k_z = 4.48$, (f) $k_z = 4.39$, (g) $k_z = 4.30$, (h) $k_z = 4.21$, (i) $k_z = 4.15$, and (j) $k_z = 4.08\,\text{Å}^{-1}$. (k) Relationship between k_x and k_z for various photon energies. The Fermi-surface maps are compared with the calculated Fermi surfaces, which are indicated by the solid curves.

around $k_z \sim 4.2\,\text{Å}^{-1}$ in the k_x-k_z plane, substantial spectral weight is observed in this region due to the flat dispersion [see Figs. 1(g)–1(j)]. The residual spectral weight at E_F due to the flat band dispersion would play an important role in the nesting picture, although the nesting vector suggested by Yang *et al.* [5] is not seen in the Fermi-surface map in the k_x-k_z plane.

In Figs. 4(a)–4(j), the ARPES intensities at E_F are plotted as functions of k_x and k_y, and the Fermi-surface maps in the k_x-k_y plane are compared with the prediction of the band structure calculations for various photon energies. The previous ARPES

study with the right-handed and left-handed polarized light showed that although the transition-matrix element strongly depends on the helicity, measurement with one of the helicities is enough to pick up all of the Fermi surfaces [15]. Here, the relationship between k_z and k_x (k_y) in Fig. 4(k) is considered in the calculation.

In going from Figs. 4(a) to 4(e), the inner and outer Fermi surfaces are relatively insensitive to the k_z value, both in the calculation and the experiment. In the calculation, the inner Fermi surface is separated from the outer one along the Γ-M line in Figs. 4(b)–4(d) and finally almost touches the outer one in Figs. 4(a) and 4(e). On the other hand, in the experiment, substantial spectral weight is observed already in Figs. 4(b)–4(d) in the region where the calculated inner and outer Fermi surfaces touch one another in Figs. 4(a) and 4(e). In going from Figs. 4(f) to 4(i), the inner and outer Fermi surfaces dramatically change with k_z, and the experimental result is basically consistent with the band structure calculation. However, substantial spectral weight is observed in the region between the calculated inner and outer Fermi surfaces.

The intervening region between the inner and outer Fermi surfaces can be related to the substantial distribution of Ir-Ir distance observed by the recent extended-x-ray absorption fine structure (EXAFS) study on $IrTe_2$ [16]. The Ir-Ir bond disorder indicates out-of-plane displacement of Ir atoms which can mix the a_{1g} and e'_g orbitals in addition to the spin-orbit interaction. Most probably, the Ir-Ir bond disorder with the out-of-plane displacement is driven by the Te-Te interaction between the layers [9] and, therefore, the Te $5p$ orbitals play important roles both in the intervening region between the Fermi surfaces and in the three dimensionality of the Fermi surfaces. Here, one can speculate that the orbital fluctuations (and the superconductivity) would be enhanced by the particular three-dimensional Fermi surfaces via the interlayer Te-Te interaction.

IV. CONCLUSION

In conclusion, we have studied the three-dimensional multiband Fermi surfaces of $Ir_{0.95}Pt_{0.05}Te_2$ using ARPES and a band structure calculation. The strong Te $5p$-Te $5p$ hybridization between the $IrTe_2$ triangular lattice layers is responsible for the strong k_z dependence of the band dispersions, which is confirmed by the ARPES experiment. The observed inner and outer Fermi surfaces with strong k_z dependence are basically consistent with the band structure calculation. The strong Te-Te interaction between the layers is responsible for the three dimensionality of the Fermi surfaces.

ACKNOWLEDGMENTS

The authors would like to thank Prof. A. Damascelli and Prof. H.-J. Noh for valuable discussions. This work was partially supported by Grants-in-Aid from the Japan Society of the Promotion of Science (JSPS) (No. 22540363, No. 25400372, No. 24740238, and No. 25400356) and the Funding Program for World-Leading Innovative R&D on Science and Technology (FIRST Program) from JSPS. T.T. and D.O. acknowledge support from the JSPS Research Fellowship for Young Scientists. The synchrotron radiation experiment was performed with the approval of Photon Factory, KEK (Project No. 2013G021).

[1] K. Horiba, K. Ono, J. H. Oh, T. Kihara, S. Nakazono, M. Oshima, O. Shiino, H. W. Yeom, A. Kakizaki, and Y. Aiura, Phys. Rev. B **66**, 073106 (2002).

[2] T. Yoshida, I. Nishi, S. Ideta, A. Fujimori, M. Kubota, K. Ono, S. Kasahara, T. Shibauchi, T. Terashima, Y. Matsuda, H. Ikeda, and R. Arita, Phys. Rev. Lett. **106**, 117001 (2011).

[3] J.-Q. Meng, P. M. Oppeneer, J. A. Mydosh, P. S. Riseborough, K. Gofryk, J. J. Joyce, E. D. Bauer, Y. Li, and T. Durakiewicz, Phys. Rev. Lett. **111**, 127002 (2013).

[4] S. Pyon, K. Kudo, and M. Nohara, J. Phys. Soc. Jpn. **81**, 053701 (2012).

[5] J. J. Yang, Y. J. Choi, Y. S. Oh, A. Hogan, Y. Horibe, K. Kim, B. I. Min, and S.-W. Cheong, Phys. Rev. Lett. **108**, 116402 (2012).

[6] N. Matsumoto, K. Taniguchi, R. Endoh, H. Takano, and S. Nagata, J. Low Temp. Phys. **117**, 1129 (1999).

[7] A. Kiswandhi, J. S. Brooks, H. B. Cao, J. Q. Yan, D. Mandrus, Z. Jiang, and H. D. Zhou, Phys. Rev. B **87**, 121107(R) (2013).

[8] D. Ootsuki, Y. Wakisaka, S. Pyon, K. Kudo, M. Nohara, M. Arita, H. Anzai, H. Namatame, M. Taniguchi, N. L. Saini, and T. Mizokawa, Phys. Rev. B **86**, 014519 (2012).

[9] A. F. Fang, G. Xu, T. Dong, P. Zheng, and N. L. Wang, Sci. Rep. **3**, 1153 (2013).

[10] Yoon Seok Oh, J. J. Yang, Y. Horibe, and S.-W. Cheong, Phys. Rev. Lett. **110**, 127209 (2013).

[11] D. Ootsuki, S. Pyon, K. Kudo, M. Nohara, M. Arita, H. Anzai, H. Namatame, M. Taniguchi, N. L. Saini, and T. Mizokawa, J. Phys. Soc. Jpn. **82**, 093704 (2013).

[12] S. Pyon, K. Kudo, and M. Nohara, Physica C **494**, 80 (2013).

[13] P. Blaha, K. Schwarz, G. K. H. Madsen, D. Kvasnicka, and J. Luitz, computer code WEIN2k (Technische Universität Wien, Austria, 2002).

[14] J. P. Perdew, K. Burke, and M. Ernzerhof, Phys. Rev. Lett. **77**, 3865 (1996).

[15] D. Ootsuki, T. Toriyama, M. Kobayashi, S. Pyon, K. Kudo, M. Nohara, T. Sugimoto, T. Yoshida, M. Horio, A. Fujimori, M. Arita, H. Anzai, H. Namatame, M. Taniguchi, N. L. Saini, T. Konishi, Y. Ohta, and T. Mizokawa, J. Phys. Soc. Jpn. **83**, 033704 (2014).

[16] B. Joseph, M. Bendele, L. Simonelli, L. Maugeri, S. Pyon, K. Kudo, M. Nohara, T. Mizokawa, and N. L. Saini, Phys. Rev. B **88**, 224109 (2013).